Materials and Design 183 (2019) 108144

Contents lists available at ScienceDirect

Materials and Design

journal homepage: www.elsevier.com/locate/matdes

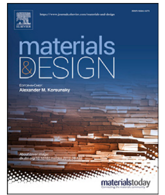

Sn-3.0Ag-0.5Cu/Sn-58Bi composite solder joint assembled using a low-temperature reflow process for PoP technology

Yu-An Shen [a,*], Shiqi Zhou [a,b], Jiahui Li [a,b], Chih-han Yang [c], Sijie Huang [a,b], Shih-kang Lin [c,d,e], Hiroshi Nishikawa [a]

[a] Joining and Welding Research Institute (JWRI), Osaka University, Ibaraki, Osaka 560-0047, Japan
[b] Graduate School of Engineering, Osaka University, Suita, Osaka 565-0871, Japan
[c] Department of Materials Science and Engineering, National Cheng Kung University, Tainan 70101, Taiwan, ROC
[d] Hierarchical Green-Energy Materials (Hi-GEM) Research Center, National Cheng Kung University, Tainan City 70101, Taiwan
[e] Center for Micro/Nano Science and Technology, National Cheng Kung University, Tainan City 70101, Taiwan

HIGHLIGHTS

- An in-situ observation was performed on a composite solder made of SAC305/Sn58Bi.
- SAC305/Sn58Bi were completely mixed by 190 °C reflow to form Sn-31.1Bi-1.4Ag-0.2Cu with a melting-like point of 176°C.
- Cu/SAC305-Sn58Bi/Cu solder joints were assembled with a shear strength of 44.6 MPa.

GRAPHICAL ABSTRACT

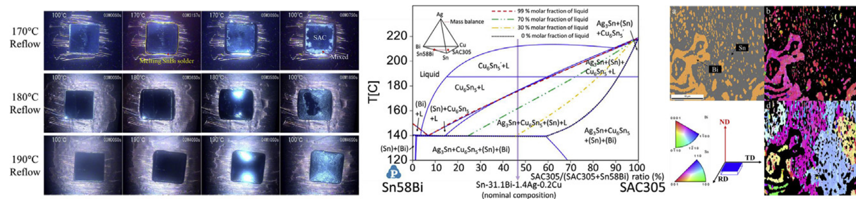

ARTICLE INFO

Article history:
Received 25 June 2019
Received in revised form
20 August 2019
Accepted 21 August 2019
Available online 22 August 2019

Keywords:
Composite solder joint
EBSD
Low-temperature soldering
Package-on-package

ABSTRACT

Package-on-Package (PoP) is a popular technology for fabricating chipsets of accelerated processing units. However, the coefficient of thermal expansion mismatch between Si chips and polymer substrates induces thermal warpage during the reflow process. As such, the reflow temperature and reliability of solder joints are critical aspects of PoP. Although Sn—58Bi is a good candidate for low-temperature processes, its brittleness causes other reliability issues. In this study, an in-situ observation was performed on composite solders (CSs) made of an Sn-3.0Ag-0.5Cu (SAC305) solder and an Sn—58Bi solder that were mixed during reflow at temperatures of 170 °C (CS-170), 180 °C (CS-180), and 190 °C (CS-190). The volumes of the mixed-solder regions were in the order of CS-190 > CS-180 > CS-170. A calculated Sn58Bi-SAC305 isoplethal section of the Sn-Ag-Cu-Bi quaternary system was employed to elucidate the melting behavior of CS-190. CS-190 with Sn cyclic twin boundary and Bi phase preferred orientation of [0001] was demonstrated by electron backscatter diffraction. Moreover, Cu/CS-190/Cu joints with a shear strength of 46 MPa were formed. CS-190 can reduce the brittleness of Sn—Bi solder owing to the reduced solid-solution hardening with the decrease in the Bi content. These factors can improve the reliability of PoP technology.

© 2019 The Authors. Published by Elsevier Ltd. This is an open access article under the CC BY-NC-ND license (http://creativecommons.org/licenses/by-nc-nd/4.0/).

1. Introduction

Decreasing power consumption and CO_2 emissions is critical for reducing manufacturing costs, and for environmental and sustainable development in the electronics industry. Thus, the role of materials and design is very important during the enhancement of performance in advanced electronic devices.

Three-dimensional integrated circuits (3D IC) have advantages such as high performance, small form factor, and heterogeneous integration, and are a promising direction to extend Moore's law [1]. Before overcoming the technological challenges in manufacturing 3D IC, Package-on-Package (PoP) technology has become popular for fabricating chipsets of accelerated processing

* Corresponding author.
E-mail address: yashen@jwri.osaka-u.ac.jp (Y.-A. Shen).

https://doi.org/10.1016/j.matdes.2019.108144
0264-1275/© 2019 The Authors. Published by Elsevier Ltd. This is an open access article under the CC BY-NC-ND license (http://creativecommons.org/licenses/by-nc-nd/4.0/).

units, wherein the top-side chip serves as the mobile memory and the bottom-side chip serves as the application processor (AP) [2,3]. In PoP, an important technology is fan-out wafer level packaging (FOWLP; developed by TSMC), which ensures a smaller package footprint with higher heterogeneous integration level and input/output density than conventional flip-chip packaging and enhanced thermal and electrical performances compared with general packaging technologies [4]. Thus, most high-performance APUs are manufactured based on PoP technology, such as the A11 APU in Apple's iPhone 8 [4]. Si chips and polymer substrates are employed in the PoP assembly process; however, the coefficient of thermal expansion (CTE) mismatch between the two materials induces serious thermal warpage during the reflow process, wherein the solders are re-melted to connect the chips and the substrates [2,5,6]. In addition, the level of thermal warpage can be reduced by controlling the reflow temperature in the range of 180 °C–200 °C [2,6]. Therefore, researchers have focused on the mechanical properties of solders and reflow temperature.

In the past few decades, despite eutectic Sn–Pb solder has a suitable melting point and performance against thermal fatigue, and thus was widely utilized for electronic packaging [7,8], it has been prohibited due to the environmental and health issues by the adoption of Restriction of Hazardous Substances Directive. On the other hand, Sn–58Bi alloy (in wt%), which has a low melting point (139 °C) and good mechanical properties, is a promising candidate for low-temperature soldering in electronic packaging [9–13]. However, its poor ductility, which is due to the considerable brittleness of Bi, is a concern [14–16], and the melting point will induce electromigration and thermomigration at low temperatures (75 °C–100 °C) [17–19].

We prepared a composite solder with an Sn-3.0Ag-0.5Cu solder (SAC305 solder, commonly used for ball-grid-array solder balls) on the top side and an Sn–58Bi solder on the bottom side at a reflow temperature lower than 250 °C–260 °C (which is the reflow temperature range for an SAC solder). During the reflow process, the bottom-side solder (i.e., Sn–58Bi) melts and then forms a mixture of the two solders. By conducting the reflow process at a temperature lower than that used for an SAC solder, we could fabricate a composite-solder joint with Cu–Cu substrates, and thus we reduced the thermal warpage and considerable thermal budget (from 250 °C–260 °C to 180–190 °C). We expect the composite solder to exhibit better ductility and a higher melting point than the Sn–58Bi solder because of the reduced Bi content. This composite solder could replace the eutectic Sn–58Bi solder for low-temperature soldering owing to the similar reflow temperature, higher working temperature, and lower content of brittle Bi. Additionally, the shear strength may be higher than that of SAC305 solder because the Bi addition can enhance the reliability of SAC-based solder [20,21].

Although similar studies have been conducted involving SAC-based solder balls with In- or Bi-Sn-based solder pastes [22–24], studies on Cu/Sn-58Bi-SAC composite solder/Cu joints, including the corresponding processes and properties during the reflow, are lacking.

In this study, the in-situ processes involved in fabricating a composite solder joints made of SAC solder/Sn-58Bi solder/Cu substrate at reflow temperatures of 170 °C, 180 °C, and 190 °C were recorded using a charge-coupled device (CCD) camera to understand the mixing behavior. The melting behavior of CS-190 was observed, and its melting-like point was predicted from thermodynamic analysis. The microstructures were investigated using a scanning electron microscope (SEM, JOEL-7100, Japan) and electron backscattered diffraction (EBSD, TSL and OIM, Japan). Furthermore, Cu/composite solder/Cu joints were assembled at a reflow temperature of 190 °C (CS-190 joint) to understand the microstructures of the joint. Finally, the soldering reliability of the joint was analyzed by conducting shear tests.

2. Experimental methods

2.1. Composite solders under various reflow temperatures

Sheets of SAC305 solder (Sn-3.0Ag-0.5Cu wt%) and Sn–58Bi (wt%) solder with dimensions of 5 mm × 5 mm × 120 μm were commercially fabricated (Senju Metal Industry Co., Ltd., Japan). A Cu plate with dimensions of 15 mm × 15 mm × 0.5 mm was prepared for the substrate. The Cu plates were cleaned in diluted hydrochloric acid (4%) followed by ethanol, resulting in Cu-oxide-free surfaces. The various reflow temperatures were 170 °C, 180 °C, and 190 °C. Fig. 1(a) shows the reflow profiles. A CCD camera was used to record the reflow processes. A composite solder (CS-190) was re-melted based on a temperature curve (ramp rate of 0.5 °C/s) from 100 °C to 220 °C, as shown in Fig. 1(b), to study the melting behavior. The microstructures of each sample were analyzed using the SEM, and the elements in the solders and intermetallic compounds (IMCs) were identified using an energy dispersive X-ray spectrometer (EDS, JOEL, Japan). EBSD was used to investigate the grain size, orientation, and grain-boundary misorientation of the Sn and Bi phases in the composite solder prepared at a reflow temperature of 190 °C. In addition, thermodynamic calculations based on the calculation of phase diagram (CALPHAD) method were performed to determine the Sn58Bi-SAC isoplethal sections of the Sn-Bi-Ag-Cu quaternary system using the PANDAT software with the ADAMIS solder database [25]. In this database, the thermodynamic descriptions of the Sn-Bi-Ag-Cu quaternary system were

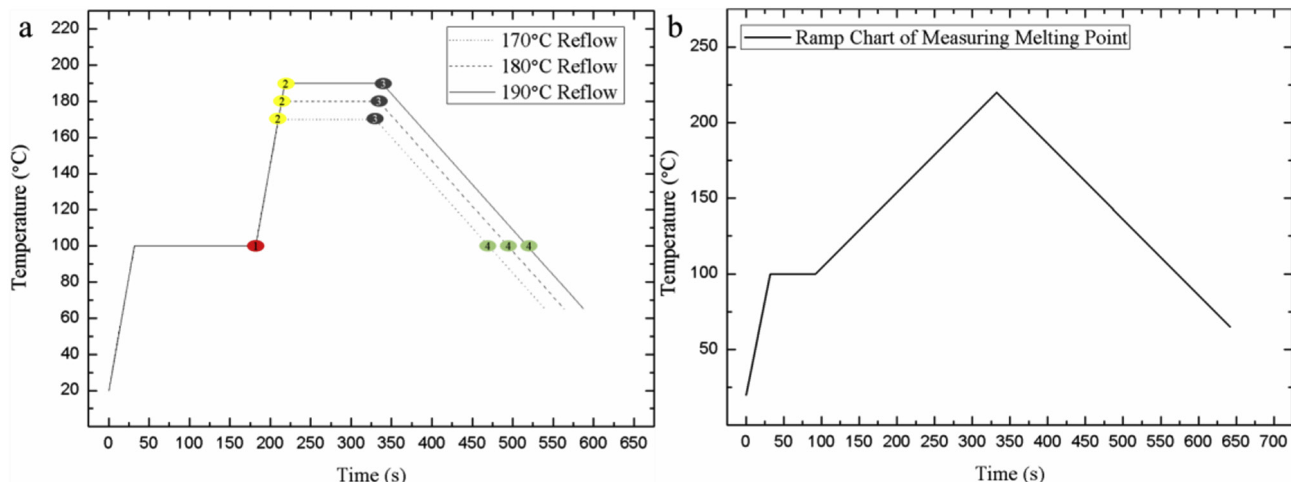

Fig. 1. (a) Reflow profiles for composite solders/Cu substrate with various reflow temperatures. (b) Ramp chart for observing the melting behavior of CS-190.

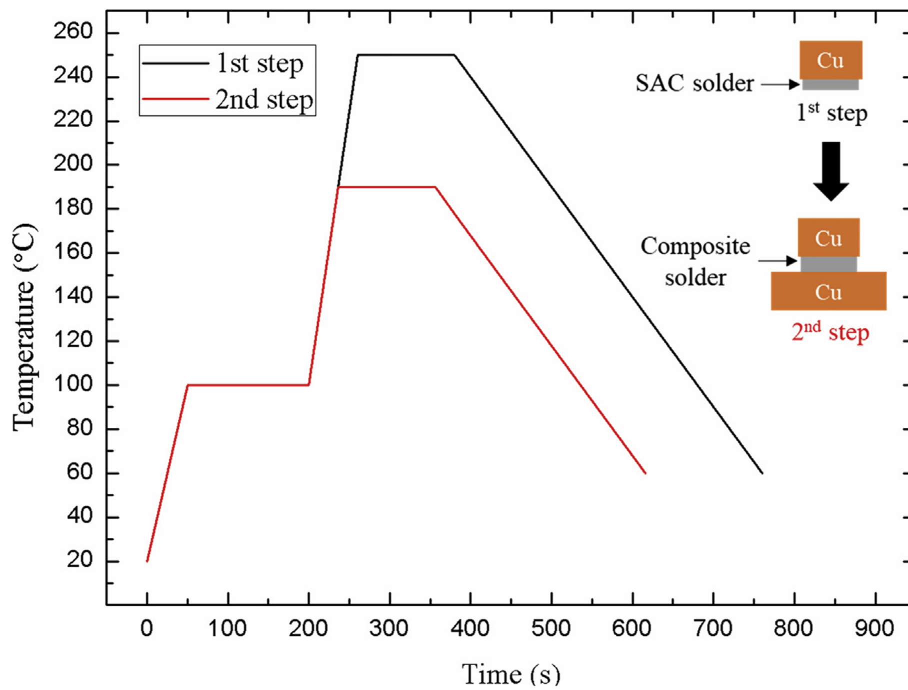

Fig. 2. Reflow profiles of the twice reflow process for assembling Cu/CS-190/Cu, with a schematic diagram of the twice reflow process.

extrapolated based on the models of Sn-Bi-Ag, Sn-Bi-Cu, Sn-Ag-Cu, and Bi-Ag-Cu ternary systems without incorporating the quaternary interacting parameters in the Gibbs free energy functions.

2.2. Cu/CS-190/Cu joints and shear strength

Fig. 2 shows the two-step reflow process conducted at temperatures of 250 °C and 190 °C. The first reflow process was for the SAC solder attached to the top-side Cu pillar; we then placed the former on a sheet of Sn—58Bi solder/bottom-side Cu pillar to assemble the Cu/composite solder/Cu joints in the second reflow process at 190 °C. In addition, the two-step reflow process was similar to the commonly used process for connecting APU chipsets with polymer substrates in PoP technology [4]. The top pillar has a thickness of 2 mm and a diameter of 5 mm, and the bottom pillar has a thickness of 5 mm and a diameter of 10 mm, as shown in Fig. 3(a). The pillars were cleaned in diluted hydrochloric acid (4%) followed by ethanol. The shear strengths were evaluated using a shear test machine (HLST1000, Rhesca, Japan) operating in the displacement-controlled mode with a shear punch offset from the substrate surface of 200 μm and a nominal displacement rate of 10 μm/s, as shown in Fig. 3(b). Three joints of the composite solder were examined for a statistical analysis.

3. Results and discussion

3.1. In-situ observations of composite solder mixing behavior during reflow

Fig. 4 shows the appearance of each sample during the reflow process in the temperature range of 170 °C—190 °C. The processes were recorded and are presented in Supplement movies 1—3. Points 1 to 4 correspond to Points 1 to Point 4 shown in Fig. 1(a). The images, shown in Fig. 4, are indicated by 170 °C-1 to 4, 180 °C-1 to 4, and 190 °C-1 to 4 for convenience. At Point 1, the solders did not melt at 100 °C. The melting of the Sn—58Bi solder started at 139 °C, which is the melting point of eutectic Sn—Bi alloys, during the temperature ramp. In 2 min at 170 °C, the SAC solder only slightly melted, indicated by 170 °C-3; at a reflow temperature of 180 °C, the SAC305 solder was considerably dissolved into the

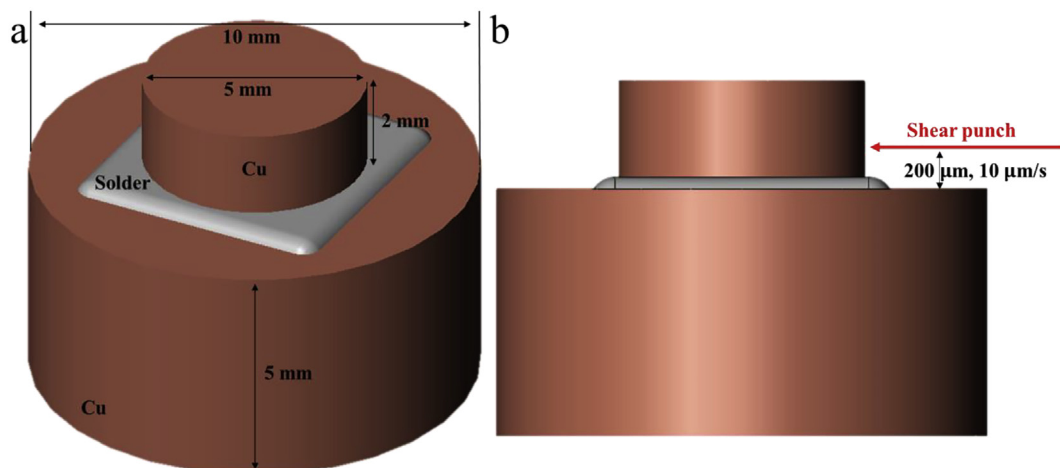

Fig. 3. (a) Dimensions of the Cu/CS-190/Cu joint and (b) test condition of the shear test.

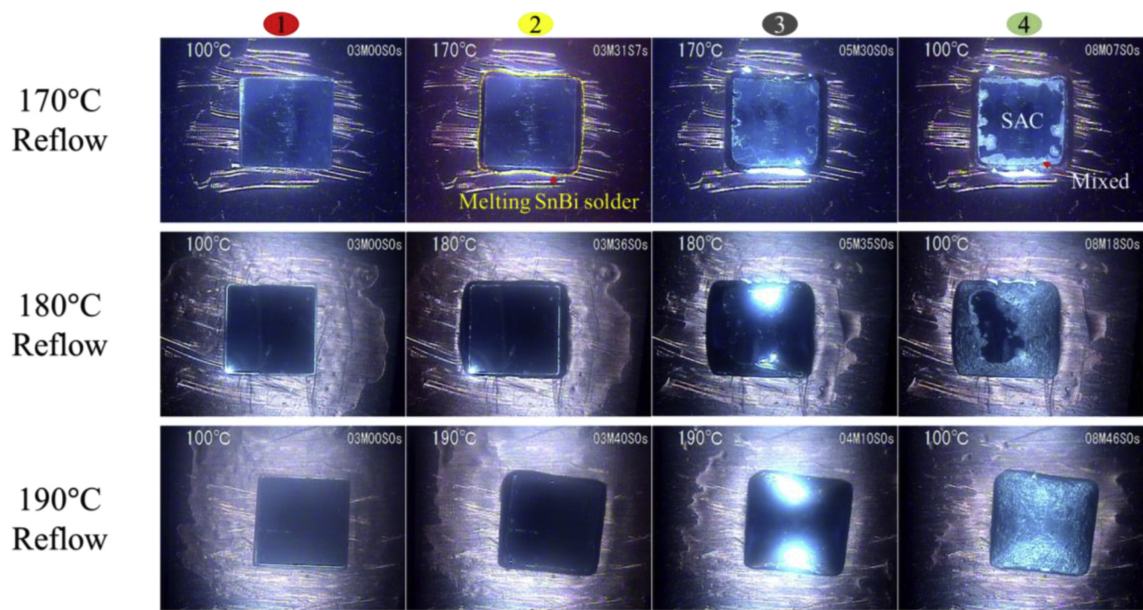

Fig. 4. Morphology of composite solders at different conditions. Point 1 to Point 4 correspond to Point 1 to Point 4 in Fig. 1(a).

Sn58Bi solder, as indicated by 180 °C-3. A completely mixed solder was formed at 190 °C, as indicated by 190 °C-3. At Point 4, the volumes of the mixed solders were in the order of 190 °C > 180 °C > 170 °C. When the solder sheet of Sn–58Bi melted, there was a layer of alloy at the interface between the Sn–58Bi and the SAC solders because of the partial dissolution of the SAC solder. The melting point of an interfacial alloy is lower than that of the SAC solder (217 °C). The dissolution is similar to transient liquid phase sintering/solid-liquid interdiffusion [26–28]. The latter formed an intermetallic compound, and the former formed a solder alloy with a melting point between Sn–58Bi and SAC solder. However, the Bi content in the Sn–58Bi solder decreased because of the dissolution of the SAC solder. At 170 °C, 180 °C, and 190 °C, the values of Sn at the liquid line were 62.5, 68.5, and 75.5 wt%, respectively, in the Sn–Bi phase diagram. Therefore, higher reflow temperature can facilitate the more dissolution of the SAC solder into the Sn–58Bi solder. With time at the peak reflow temperature, the SAC solder dissolves into the molten solder of the Sn–58Bi alloy until the Bi content of the mixed solder reaches the Bi wt% at the liquid line in the Sn–Bi phase diagram. Fig. 5 shows a schematic of the solder mixing process. The Bi contents in the mixed solders are presented in Section 3.2.

However, we believe that the completely mixed solder is the best structure for PoP technology because the interface of the SAC and SnBi solder induces a decline in the mechanical properties. In this study, we only focused on the melting behavior of the composite solder reflowing at 190°C (CS-190). Although the process is conducted at 190 °C, the SAC305 melting point is ~217 °C. Thus, we heated to 210 °C, a little lower than 217 °C, to identify the real melting-like point. The CS-190 was observed by in-situ recording at a ramp rate of 0.5 °C/s from 100 °C to 210 °C, as shown in Fig. 6 and Supplement Movie 4. When the temperature was above 140 °C, which is close to the melting point of eutectic Sn–Bi alloy, the solder gradually melted before completely melting at 190 °C, at which point its structure was similar to that at 210 °C. Most solid phases were eliminated from the molten state solder in the temperature range of 170 °C to 180 °C. Thus, we can conclude that the melting point is approximately in the range of 170 °C–190 °C.

Fig. 7 shows the Sn58Bi-SAC305 isoplethal section, with a Ag-Bi-Cu-Sn tetrahedron highlighting the two terminal compositions of the phase diagram. The 99%, 70%, 30%, and 0% iso-liquid phase fraction lines and nominal composition of the composited solder were superimposed on the phase diagram. At elevated temperatures (e.g., 170 °C–190 °C in this work), the Sn58Bi portion of the composite solder is completely molten, while the other portion of the SAC305 is composed of (Sn), Cu_6Sn_5, and Ag_3Sn solid phases. Between the Sn58Bi and SAC305 terminals, there is a wide range in the $Cu_6Sn_5' + L$ or $Cu_6Sn_5 + L$ two-phase region; however, the solid phase (Cu_6Sn_5 or Cu_6Sn_5') fraction in this region is very small, <1%, as indicated by the 99% iso-liquid phase fraction line. That is why the structure of CS-190 at 190°C is similar to that at 210°C (Fig. 6). A noticeable decrease in liquid phase fraction occurs when the Ag_3Sn and (Sn) phases participate in the solidification of the $Cu_6Sn_5' + Ag_3Sn + (Sn) + L$ and $Cu_6Sn_5 + Ag_3Sn + (Sn) + L$ four-phase regions. Consequently, the 99% iso-liquid phase fraction line is taken as the criterion for evaluating the melting behavior of the composite solder. The Sn58Bi/SAC305 contact would result in mutual dissolution and diffusion. Since the kinetics in the liquid phase is an order-of-magnitude higher than that in solid phases, the predominant reactions would occur at the liquid phase. With

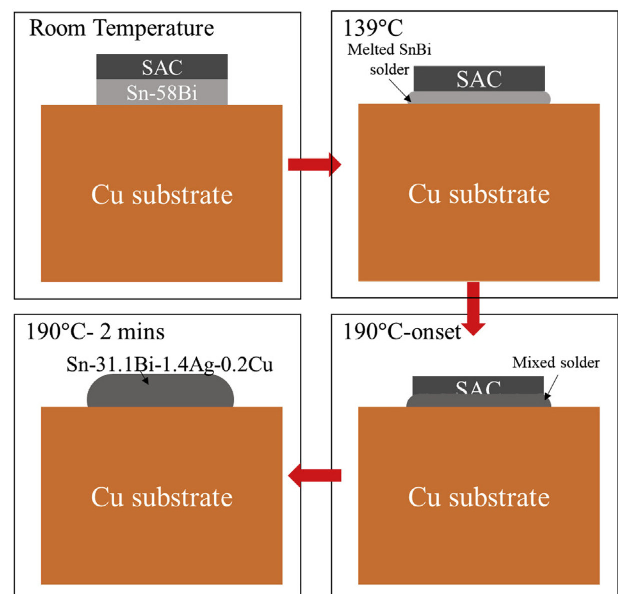

Fig. 5. Schematic diagram of the mixing process of composite solder.

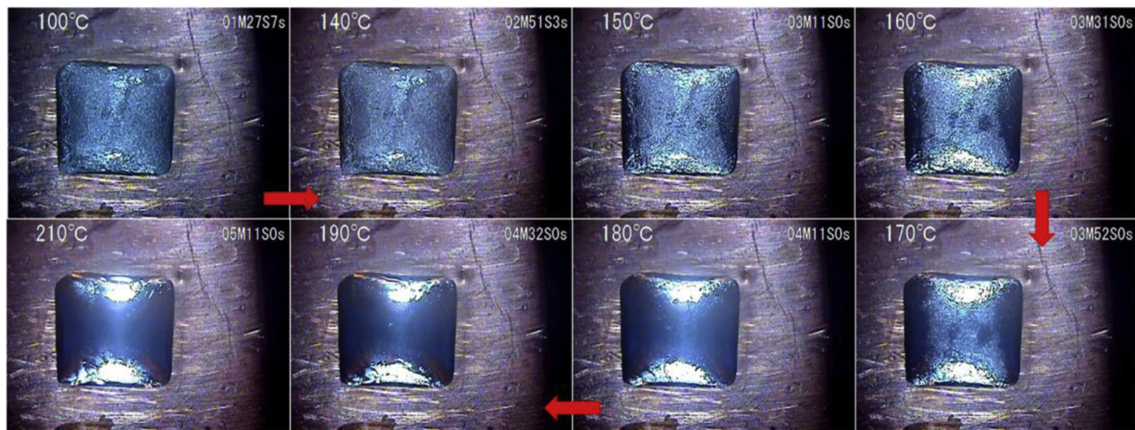

Fig. 6. Frames extracted from Supplement Movie 4 for observing the melting behavior of CS-190.

the dissolution of SAC305 constituents into the molten Sn58Bi alloy at elevated temperatures, the molten part of the composite solder can retain its liquid phase with the SAC305/(Sn58Bi + SAC305) ratios being 39.7%, 51.0%, and 62.7% at 170 °C, 180 °C, and 190 °C, respectively. The higher the reflow temperature, the more extensive the range of SAC305 dissolution in the liquid phase, which is consistent with the experimental results shown in Fig. 4. Complete mixing of Sn58Bi and SAC305 composite solder in this work resulted in the formation of Sn-31.1Bi-1.4Ag-0.2Cu alloy, which has a 99% liquid phase temperature at approximately 176 °C. Although this is not the melting point, it can be defined as a melting-like point because the Cu_6Sn_5 content in CS-190 is low. The working temperature of CS-190, which was fabricated based on the reflow profile of the low-temperature Sn—58Bi alloy, can be higher than that of the Sn—58Bi solder (melting point is 139 °C) because of its melting-like point at approximately 176 °C. This is beneficial for enhancing the electromigration and thermomigration reliabilities. Moreover, this process can lower the considerable thermal budget compared with the SAC solder case (reflow temperature is 250 °C) and avoid the thermal warpage observed during the high-temperature reflow process.

3.2. Microstructure of composite solders

Fig. 8 shows cross-sectional backscattered electron images (BEIs) of CS-170, CS-180, and CS-190. There is a boundary between the SAC-solder region and the mixed-solder region in CS-170 (Fig. 8a) and CS-180 (Fig. 8b), but not in CS-190 (Fig. 8c). The results correspond to the difference in the SAC-solder volumes shown in Fig. 4. With the increase in the reflow temperature, the higher rate of dissolution of the SAC solder into the Sn—58Bi solder induces thicker mixed regions in CS-180 (Fig. 8b) than in CS-170 (Fig. 8a) and completely mixed regions in CS-190 (Fig. 8c). In Fig. 4, the areas of the SAC solder are 0.18 and 0.056 cm^3 in 170 °C-4 and 180 °C-4, respectively. The thicknesses of the SAC-solder region in CS-170 and CS-180 are approximately 72.1 and 12.1 μm, respectively. Therefore, the values of Bi in the mixed solders are 38.9 and 31.4 wt% after the reflow at 170 °C and 180 °C, respectively. These

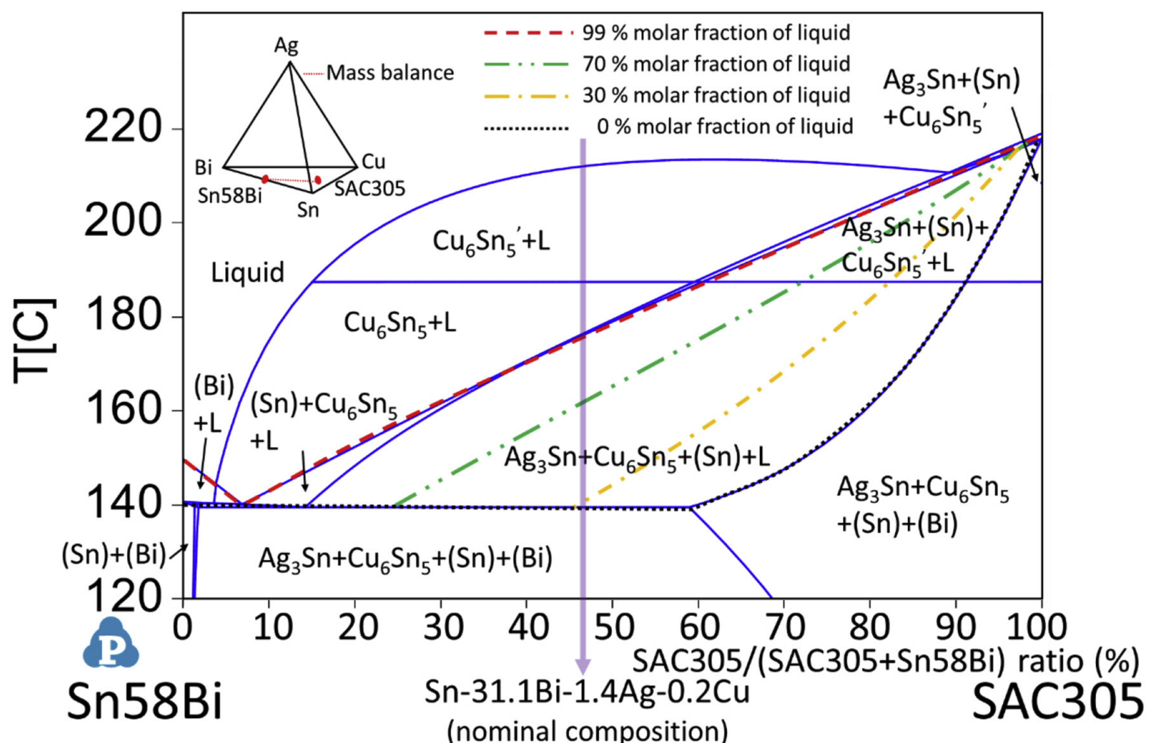

Fig. 7. Sn58Bi-SAC305 isoplethal section superimposed with 99%, 70%, 30%, and 0% molar fractions of liquid.

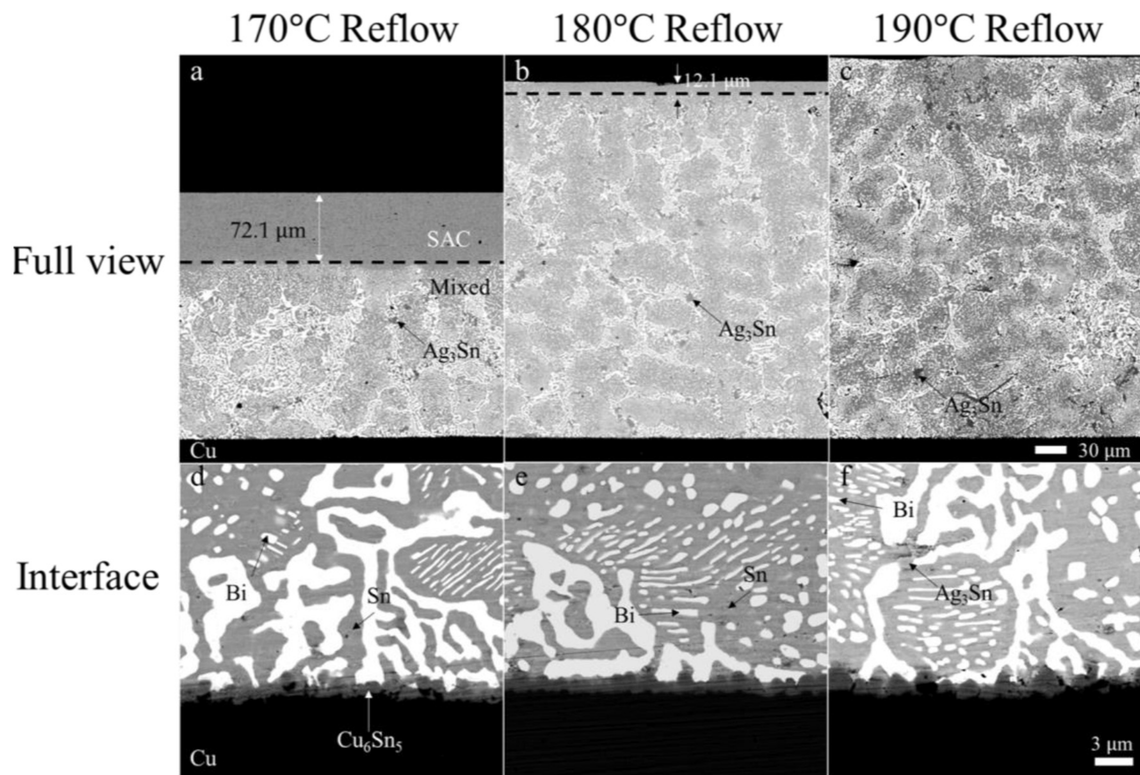

Fig. 8. Cross-section microstructures in composite solder of (a) CS-170, (b) CS-180, and (c) CS-190, and amplified backscatter electron images (BEIs) of (d) CS-170, (e) CS-180, and (f) focusing on the interfaces between the solder and the Cu substrate.

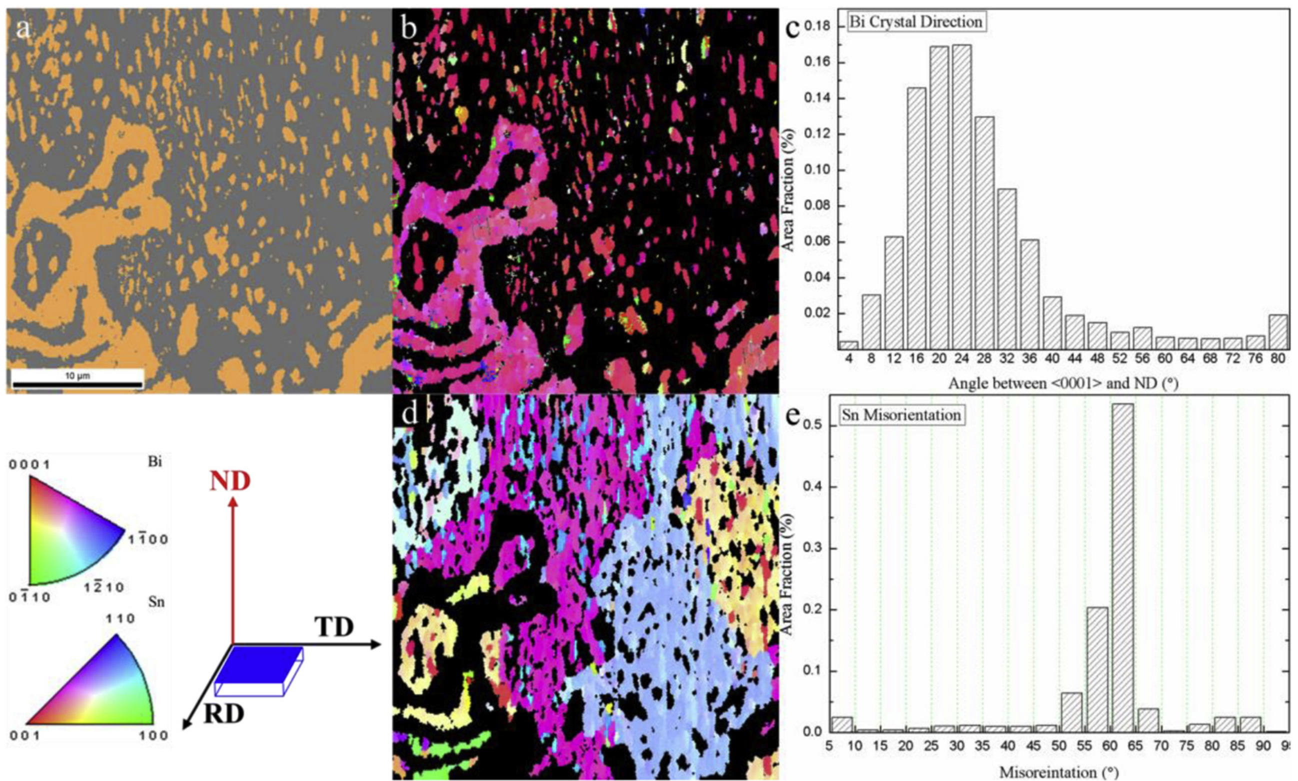

Fig. 9. Electron backscatter diffraction (EBSD) of Sn and Bi IPF in ND. (a) EBSD phase mapping. EBSD mapping of (b) Bi and (d) Sn. Distribution of (c) angle between ⟨0001⟩ and ND in Bi crystal and (e) misorientation in Sn grain boundaries.

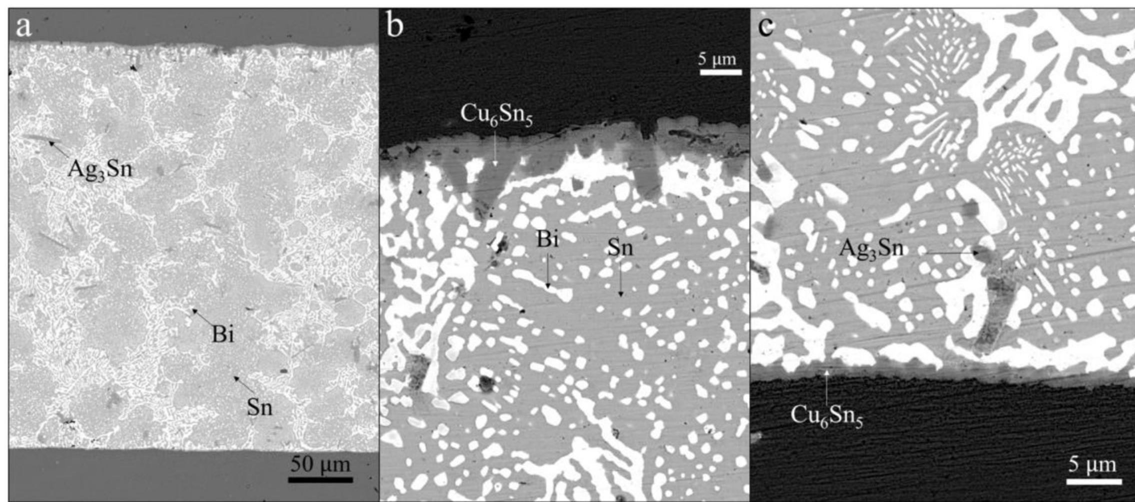

Fig. 10. Cross-sectional BEIs in (a) full-view, and at the interface between (b) the top Cu substrate and (c) bottom Cu substrate in the CS-190 joint.

values are very close to the Bi contents at the liquidus at 170 °C (37.5 wt% Bi) and 180 °C (31.2 wt% Bi) in the Sn–Bi phase diagram [29].

In the Sn–58Bi solder, the phase transition through the eutectic point results in a uniform lamellar structure [30–32]. Conversely, in CS-190, smaller Bi grains precipitate from the primary crystal of Sn during the cooling process between its melting point and 139 °C (eutectic point of Sn–Bi). A net-like structure is formed in the composite Sn–Bi alloy during solidification (Fig. 8c). Therefore, the distribution of the Bi phase in the composite solder is distinct from that in the Sn–58Bi solder. In the latter, the Bi and Sn phases form uniform lamellae; however, a net-like structure is observed in the former, instead of the uniform lamellae in the latter, because of the reduction in the Bi content to 31.1 wt% during the mixing of the SAC and eutectic Sn–58Bi solders, as shown in Fig. 8(a)–(c), and considerably small Bi grains precipitate from the Sn phase, as shown in Fig. 8(d)–(f). When only a small amount of SAC is dissolved into the Sn–58Bi solder (Fig. 8a), fewer net-like structures are observed in the mixed region. As thermal-stress crowding occurred on the phase boundaries of Sn–Bi [33], the net-like structures could be beneficial to the thermomechanical properties of Sn–Bi alloys. Additionally, the interfacial layer between the composite solder and the Cu substrates is made of a Cu–Sn IMC because Bi–Cu IMC does not exist.

Plane-view microstructures of CS-190 were examined using EBSD. Fig. 9(a) shows phase mapping (80 μm × 80 μm) of CS-190. Fig. 9(b) and (d) show the orientation image mapping (OIM) of Bi and Sn, respectively. Cyclic twin boundaries (CTB), which are commonly observed in Sn-rich solders [34], exist in the Sn phase of CS-190, as shown in Fig. 9(e). In a previous study [33], CTBs in the Sn phase were also observed in eutectic Sn–58Bi solder despite only 42% Sn content. In this study, CS-190, consisting of Sn-31.1Bi-1.4Ag-0.2Cu, has a more content of Sn than eutectic Sn–58Bi solder. Thus, that there are CTBs in the Sn phase of Sn-31.1Bi-1.4Ag-0.2Cu solder is reasonable. As atomic diffusion along the Sn grain boundary during electromigration causes substrate dissolution in Sn-rich solder joints, the resistance provided by the CTB against grain-boundary diffusion is very important for the electromigration reliability of CS-190 [35].

On the other hand, Sn with a body-centered tetragonal structure and Bi with a rhombohedral structure have anisotropic properties, such as anisotropic diffusivity and anisotropic CTE [36–39]. Therefore, the grain orientation in the Sn and Bi phases is critical. Interestingly, in the normal direction, Bi has a preferred orientation of [0001] (Fig. 9c), which results in a greater CTE difference from the a-axis of the Bi phase [38], and the distribution of the Sn grain orientation is random (Fig. 9d). The Bi preferred orientation of [0001] was also observed in the eutectic Sn–58Bi alloy [33]. We inferred that the Bi preferred orientation [0001] is an absolute structure in Sn–Bi alloy for minimizing the system free energy during crystallization. Although the detailed mechanism needs to be investigated in more details, this finding provides a good reference for understanding the thermomechanical properties of composite solders because the CTE of Bi is anisotropic.

3.3. Cu/composite solder/Cu solder joint

After understanding the mixing behavior of the composite solders, we assembled Cu/composite solder/Cu joints based on the reflow profile at 190 °C; the solders were mixed completely. Fig. 10(a) shows a cross-sectional BEI of the CS-190 joint. A completely mixed solder with a Sn–Bi distribution of net-like structures was observed, similar to the CS-190 solder shown in Fig. 10(c). The formation of a Cu–Sn IMC at both the interfaces between the Cu substrates and the solder is identified using EDS. Fig. 10(b) and (c) show the BEIs near the top and bottom interfaces between the Cu substrate and the solder, respectively.

The cross-sectional areas of IMC in Fig. 10 were measured. Three

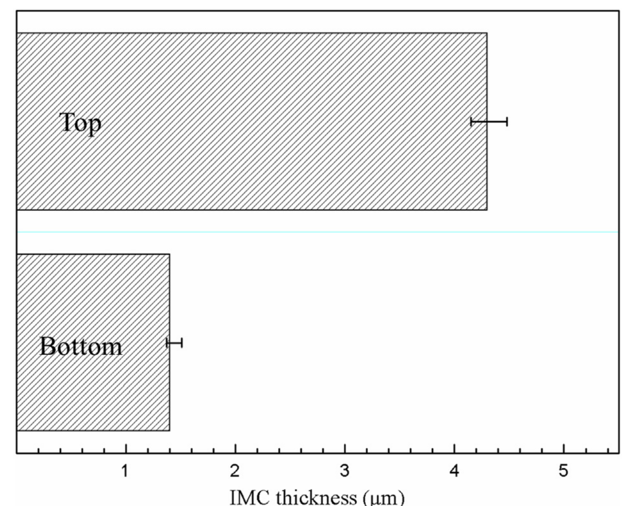

Fig. 11. Intermetallic compound (IMC) thickness at the interfaces of the top (twice reflow) and bottom (one-time reflow) of the CS-190 joint.

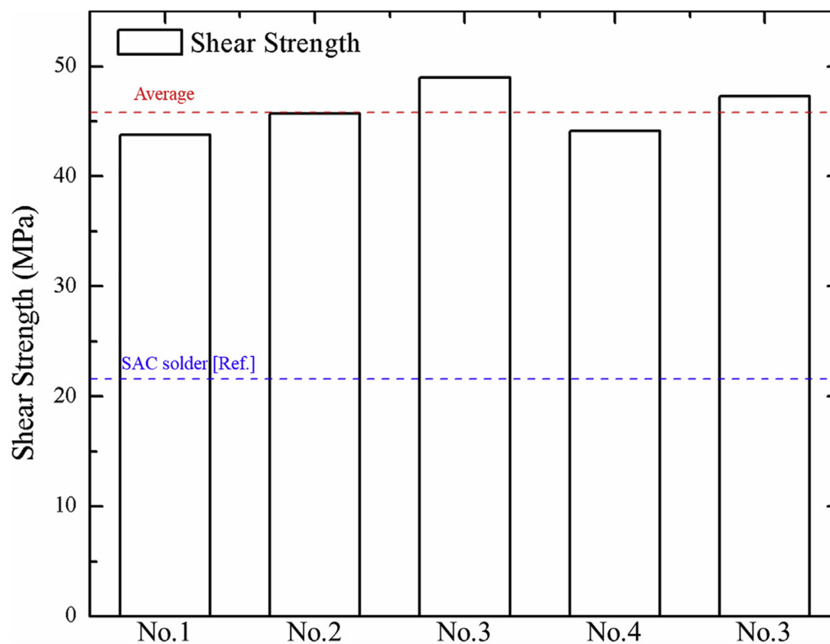

Fig. 12. Shear strengths of five CS-190 joint samples with their average strength (red dash) compared with that of SAC (blue dash, [37]) solder joints for reference. (For interpretation of the references to color in this figure legend, the reader is referred to the web version of this article.)

different 30-μm-wide regions were measured at each side. Then, the areas were divided by the width (30 μm) to calculate the IMC thicknesses. The IMC layer at the top side (4.3 μm) was thicker than that at the bottom side (1.4 μm), as shown in Fig. 11. This is due to the dual reflow to the top interface where thicker Cu_6Sn_5 IMC exists compared with that at the bottom interface, which was produced via a single reflow.

In electronic packaging, solder joints form not only an electrical interconnection but also a mechanical interconnection between the chips and the substrates. Thus, it is necessary to investigate the shear strength of the CS joints. Fig. 12 lists the shear strengths of CS-190 joints. The average shear strength (46 MPa) is much higher than that of the SAC solder joints (23 MPa) [40], which are commonly used in electronic packaging. If the Bi content in Sn—Bi alloys is in the range of 30—40 wt%, the solder will exhibit high elongation owing to the reduced solid-solution hardening effect on the Sn—Bi mechanical properties [41,42]. In our study, the Bi content was 31.1 wt% in the CS-190 joint, which could reduce brittleness in the Sn—Bi solder joint.

During reflow, serious thermal warpage is observed in the PoP assembly process because of the CTE mismatch between the Si chip and the polymer substrate. Thus, the mechanical reliability and the melting point of the solder joint are important parameters. The CS-190 joint assembled in this study at a low reflow temperature (190 °C), which has good shear strength and less brittle Bi than Sn—58B solders, is expected to be a promising candidate for PoP technology. Furthermore, as the melting point is higher than that of Sn—58Bi solder, it could enhance the working temperature of electronic devices.

4. Conclusions

The mixing processes of composite solders made of an SAC solder and a Sn—58Bi solder mixed at reflow temperatures of 170 °C, 180 °C, and 190 °C were demonstrated using in-situ observation. The volumes of the mixed solders were in the order of CS-190 > CS-180 > CS-170, which is consistent with the thicknesses of the SAC solder regions of CS-170 (72.1 μm), CS-180 (12.1 μm), and CS-190 (complete mixing). The thickness difference was due to the difference in the rate of dissolution of the SAC solder into the melted Sn—58Bi solder at higher reflow temperatures. In addition, the melting behavior of CS-190 was observed using a CCD camera at a ramp rate of 0.5 °C/s from 100 °C to 210 °C, and a melting-like point of 176 °C was determined from the Sn58Bi-SAC305 isoplethal section, indicating that the working temperature of CS-190 is higher than that of the Sn—58Bi solder (melting point = 139 °C). A net-like structure of Sn—Bi formed in CS-190 as it solidified; this is completely different from the structure of uniform lamellae observed in eutectic Sn—58Bi solder. EBSD analysis revealed that CS-190 exhibits Sn CTB and that the preferred orientation of the Bi phase is [0001]. Via a two-step reflow process, we assembled Cu/composite solder/Cu solder joints at a reflow temperature of 190 °C. The shear strength (46 MPa) of the CS-190 joint was higher than that of the SAC solder joint. Meanwhile, the brittleness of CS-190 with the decrease in the Bi content could be lower than that of eutectic Sn—58Bi solder owing to the reduced solid-solution hardening. The findings reveal that a low-temperature reflow process (190 °C) helps reduce the considerable thermal budget and thermal warpage due to the CTE mismatch between the Si chip and the polymer substrate during the reflow process in PoP technology.

Supplementary data to this article can be found online at https://doi.org/10.1016/j.matdes.2019.108144.

CRediT authorship contribution statement

Yu-An Shen: Conceptualization, Investigation, Methodology, Formal analysis, Writing - original draft, Writing - review & editing, Visualization.**Shiqi Zhou:**Investigation, Methodology.**Jiahui Li:**Investigation, Methodology.**Chih-han Yang:**Investigation, Methodology.**Sijie Huang:**Investigation, Methodology.**Shih-kang Lin:**Formal analysis, Writing - review & editing.**Hiroshi Nishikawa:**Funding acquisition, Writing - review & editing, Supervision.

Acknowledgement

This work was financially supported by Project to Create Research and Educational Hubs for Innovative Manufacturing in Asia, Osaka University of Special Budget Project by the Ministry of

Education, Culture, Sports, Science and Technology (MEXT). S.K.L and C.H.Y. gratefully acknowledge the financial support from the Ministry of Science and Technology of Taiwan (MOST) (106-2628-E-006-002-MY3).

References

[1] K.N. Tu, Reliability challenges in 3D IC packaging technology, Microelectron. Reliab. 51 (2011) 517–523, https://doi.org/10.1016/J.MICROREL.2010.09.031.

[2] A. Yoshida, Jun Taniguchi, K. Murata, M. Kada, Y. Yamamoto, Y. Takagi, T. Notomi, A. Fujita, A study on package stacking process for package-on-package (PoP), in: 56th Electron. Components Technol. Conf. 2006, IEEE, n.d.: pp. 825–830. doi:https://doi.org/10.1109/ECTC.2006.1645753.

[3] Y. Lin, C. Kang, L. Chua, W.K. Choi, S.W. Yoon, Advanced 3D eWLB-PoP (embedded wafer level ball grid array-package on package) technology, in: Proc. - Electron. Components Technol. Conf. 2016-Augus, 2016, pp. 1772–1777, https://doi.org/10.1109/ECTC.2016.257.

[4] J.H. Lau, FOWLP: PoP, in: Fan-out Wafer-Level Packag, Springer Singapore, Singapore, 2018, pp. 207–216, https://doi.org/10.1007/978-981-10-8884-1_8.

[5] S.Y. Yang, Y.D. Jeon, S.B. Lee, K.W. Paik, Solder reflow process induced residual warpage measurement and its influence on reliability of flip-chip electronic packages, Microelectron. Reliab. 46 (2006) 512–522, https://doi.org/10.1016/j.microrel.2005.06.007.

[6] C. Chen, F. Hou, F. Liu, Q. She, L. Cao, L. Wan, Thermo-mechanical reliability analysis of a RF SiP module based on LTCC substrate, Microelectron. Reliab. 79 (2017) 38–47, https://doi.org/10.1016/J.MICROREL.2017.10.003.

[7] M.N. Collins, J. Punch, R. Coyle, M. Reid, R. Popowich, P. Read, D. Fleming, Thermal fatigue and failure analysis of SnAgCu solder alloys with minor Pb additions, IEEE Trans. Components, Packag. Manuf. Technol. 1 (2011) 1594–1600, https://doi.org/10.1109/TCPMT.2011.2150223.

[8] C. Chen, H.-Y. Hsiao, Y.-W. Chang, F. Ouyang, K.N. Tu, Thermomigration in solder joints, Mater. Sci. Eng. R Reports. 73 (2012) 85–100, https://doi.org/10.1016/J.MSER.2012.11.001.

[9] Z. Mei, J.W. Morris, Characterization of eutectic Sn-Bi solder joints, J. Electron. Mater. 21 (1992) 599–607, https://doi.org/10.1007/BF02655427.

[10] H.F. Zou, Q.K. Zhang, Z.F. Zhang, Eliminating interfacial segregation and embrittlement of bismuth in SnBi/Cu joint by alloying Cu substrate, Scr. Mater. 61 (2009) 308–311, https://doi.org/10.1016/j.scriptamat.2009.04.009.

[11] S. Zhou, O. Mokhtari, M.G. Rafique, V.C. Shunmugasamy, B. Mansoor, H. Nishikawa, Improvement in the mechanical properties of eutectic Sn58Bi alloy by 0.5 and 1 wt% Zn addition before and after thermal aging, J. Alloys Compd. 765 (2018) 1243–1252, https://doi.org/10.1016/J.JALLCOM.2018.06.121.

[12] G. Ren, M.N. Collins, Improved reliability and mechanical performance of ag microalloyed Sn58Bi solder alloys, Metals (Basel) 9 (2019) 462, https://doi.org/10.3390/met9040462.

[13] G. Ren, I.J. Wilding, M.N. Collins, Alloying influences on low melt temperature SnZn and SnBi solder alloys for electronic interconnections, J. Alloys Compd. 665 (2016) 251–260, https://doi.org/10.1016/J.JALLCOM.2016.01.006.

[14] L.E. Felton, C.H. Raeder, D.B. Knorr, The Properties of Tin-Bismuth Alloy Solders, n.d. https://link.springer.com/content/pdf/10.1007%2FBF03222377.pdf (accessed August 20, 2019).

[15] L. Yang, W. Zhou, Y. Ma, X. Li, Y. Liang, W. Cui, P. Wu, Effects of Ni addition on mechanical properties of Sn58Bi solder alloy during solid-state aging, Mater. Sci. Eng. A 667 (2016) 368–375, https://doi.org/10.1016/j.msea.2016.05.015.

[16] S. Zhou, Y.-A. Shen, T. Uresti, V.C. Shunmugasamy, B. Mansoor, H. Nishikawa, Improved mechanical properties induced by In and In & Zn double additions to eutectic Sn58Bi alloy, J. Mater. Sci. Mater. Electron. (2019) 1–12, https://doi.org/10.1007/s10854-019-01056-y.

[17] X. Gu, Y.C. Chan, Thermomigration and electromigration in Sn58Bi solder joints, J. Appl. Phys. 105 (2009), 093537, https://doi.org/10.1063/1.3125458.

[18] X. Gu, Y.C. Chan, Electromigration in line-type Cu/Sn-Bi/Cu solder joints, J. Electron. Mater. 37 (2008) 1721–1726, https://doi.org/10.1007/s11664-008-0539-8.

[19] Y.-A. Shen, S. Zhou, J. Li, K.N. Tu, H. Nishikawa, Thermomigration induced microstructure and property changes in Sn-58Bi solders, Mater. Des. (2019), https://doi.org/10.1016/j.matdes.2019.107619.

[20] M.N. Collins, E. Dalton, J. Punch, Microstructural influences on thermo-mechanical fatigue behaviour of third generation high Ag content Pb-Free solder alloys, J. Alloys Compd. 688 (2016) 164–170, https://doi.org/10.1016/J.JALLCOM.2016.07.191.

[21] E. Dalton, G. Ren, J. Punch, M.N. Collins, Accelerated temperature cycling induced strain and failure behaviour for BGA assemblies of third generation high Ag content Pb-free solder alloys, Mater. Des. 154 (2018) 184–191, https://doi.org/10.1016/J.MATDES.2018.05.030.

[22] O.H. Chen, J. Gao, T.C.C. Pan, K. Kwan Tang, R. Aspandiar, K. Byrd, S. Mokler, A. Molina, Solder joint reliability on mixed sac-bisn ball grid array solder joints formed with resin reinforced bi-sn metallurgy solder pastes, in: Proc. SMTA Int, 2016, pp. 216–228. http://www.circuitinsight.com/pdf/Solder_Joint_Reliability_Mixed_SAC-BISN_Ball_Grid_Array_Solder_Joints_Formed_With_Resin_Reinforced_BI-SN_Metallurgy_SolderPastes_smta.pdf. (Accessed 27 April 2019).

[23] S.-W. Chen, S.-K. Lin, C.-F. Yang, Interfacial reactions in the pb-free composite solders with indium layers, J. Electron. Mater. 35 (2006) 72–75, https://doi.org/10.1007/s11664-006-0186-x.

[24] Y. Liu, R. Xu, H. Zhang, F. Sun, Microstructure and shear behavior of solder joint with Sn58Bi/Sn3.0Ag0.5Cu/Cu superposition structure, J. Mater. Sci. Mater. Electron. (2019) 1–8, https://doi.org/10.1007/s10854-019-01773-4.

[25] W. Cao, S.-L. Chen, F. Zhang, K. Wu, Y. Yang, Y.A. Chang, R. Schmid-Fetzer, W.A. Oates, PANDAT software with PanEngine, PanOptimizer and Pan-Precipitation for multi-component phase diagram calculation and materials property simulation, Calphad 33 (2009) 328–342, https://doi.org/10.1016/J.CALPHAD.2008.08.004.

[26] D.M. Turriff, S.F. Corbin, Modelling the influences of solid-state interdiffusion and dissolution on transient liquid phase sintering kinetics in a binary isomorphous system, Metall. Mater. Trans. A. 37 (2006) 1645–1655, https://doi.org/10.1007/s11661-006-0106-y.

[27] Y.S. Chiu, H.Y. Yu, H.T. Hung, Y.W. Wang, C.R. Kao, Phase formation and microstructure evolution in Cu/In/Cu joints, Microelectron. Reliab. 95 (2019) 18–27, https://doi.org/10.1016/J.MICROREL.2019.02.004.

[28] C.A. Yang, S. Yang, X. Liu, H. Nishikawa, C.R. Kao, Enhancement of nano-silver chip attachment by using transient liquid phase reaction with indium, J. Alloys Compd. 762 (2018) 586–597, https://doi.org/10.1016/J.JALLCOM.2018.05.254.

[29] T.B. Massalski, H. (Hiroaki) Okamoto, ASM International., Binary Alloy Phase Diagrams, ASM International, 1990. https://www.asminternational.org/online-catalog/alloy-phase-diagrams/-/journal_content/56/10192/57718G/PUBLICATION (accessed April 27, 2019).

[30] Y. Ma, X. Li, W. Zhou, L. Yang, P. Wu, Reinforcement of graphene nanosheets on the microstructure and properties of Sn58Bi lead-free solder, Mater. Des. 113 (2017) 264–272, https://doi.org/10.1016/j.matdes.2016.10.034.

[31] S. Zhou, C. Yang, Y.-A. Shen, S. Lin, H. Nishikawa, The newly developed Sn–Bi–Zn alloy with a low melting point, improved ductility, and high ultimate tensile strength, Materialia 6 (2019), 100300, https://doi.org/10.1016/J.MTLA.2019.100300.

[32] S.B. Liang, C.B. Ke, J.Q. Huang, M.B. Zhou, X.P. Zhang, Phase field simulation of microstructural evolution and thermomigration-induced phase segregation in Cu/Sn58Bi/Cu interconnects under isothermal aging and temperature gradient, Microelectron. Reliab. 92 (2019) 1–11, https://doi.org/10.1016/J.MICROREL.2018.11.007.

[33] Y.-A. Shen, S. Zhou, H. Nishikawa, Preferred orientation of Bi and effect of Sn-Bi microstructure on mechanical and thermomechanical properties in eutectic Sn-Bi alloy, Materialia 6 (2019), 100309, https://doi.org/10.1016/J.MTLA.2019.100309.

[34] L.P. Lehman, Y. Xing, T.R. Bieler, E.J. Cotts, Cyclic twin nucleation in tin-based solder alloys, Acta Mater. 58 (2010) 3546–3556, https://doi.org/10.1016/j.actamat.2010.01.030.

[35] Y.-A. Shen, C. Chen, Effect of Sn grain orientation on formation of Cu6Sn5 intermetallic compounds during electromigration, Scr. Mater. 128 (2017) 6–9, https://doi.org/10.1016/j.scriptamat.2016.09.028.

[36] B.F. Dyson, T.R. Anthony, D. Turnbull, Interstitial diffusion of copper in tin, J. Appl. Phys. 38 (1967) 3408, https://doi.org/10.1063/1.1710127.

[37] D.A. Shnawah, M.F.M. Sabri, I.A. Badruddin, A review on thermal cycling and drop impact reliability of SAC solder joint in portable electronic products, Microelectron. Reliab. 52 (2012) 90–99, https://doi.org/10.1016/j.microrel.2011.07.093.

[38] B. Arnaud, S. Lebègue, G. Raffy, Anisotropic thermal expansion of bismuth from first principles, Phys. Rev. B 93 (2016), 094106, https://doi.org/10.1103/PhysRevB.93.094106.

[39] Y.-A. Shen, F.-Y. Ouyang, C. Chen, Effect of Sn grain orientation on growth of Cu-Sn intermetallic compounds during thermomigration in Cu-Sn2.3Ag-Ni microbumps, Mater. Lett. 236 (2019) 190–193, https://doi.org/10.1016/j.matlet.2018.10.112.

[40] S.M.L. Nai, J. Wei, M. Gupta, Interfacial intermetallic growth and shear strength of lead-free composite solder joints, J. Alloys Compd. 473 (2009) 100–106, https://doi.org/10.1016/J.JALLCOM.2008.05.070.

[41] H. Takao, A. Yamada, H. Hasegawa, Mechanical Properties and Solder Joint Reliability of Low-melting Sn-Bi-Cu Lead Free Solder Alloy. https://www.tytlabs.com/japanese/review/rev392pdf/392_049takao.pdf, 2011.

[42] L. Shen, P. Septiwerdani, Z. Chen, Elastic modulus, hardness and creep performance of SnBi alloys using nanoindentation, Mater. Sci. Eng. A 558 (2012) 253–258, https://doi.org/10.1016/J.MSEA.2012.07.120.